1

A Posteriori Error Estimation and Mesh Adaptivity for Finite Volume and Finite Element Methods

Timothy J. Barth

NASA Ames Research Center, Moffett Field, CA 94035, USA
barth@nas.nasa.gov

Published in Springer series Lecture Notes in Computational Science and Engineering (LNCSE), Vol 41, 2004

Summary. Error representation formulas and *a posteriori* error estimates for numerical solutions of hyperbolic conservation laws are considered with specialized variants given for the Godunov finite volume and discontinuous Galerkin finite element methods. The error representation formulas utilize the solution of a dual problem to capture the nonlocal error behavior present in hyperbolic problems. The error representation formulas also provide a framework for understanding superconvergence properties of functionals and fundamental differences between finite element and Godunov finite volume methods. Computable error estimates are then constructed for practical implementation in computer codes. The error representation formulas and computable error estimates also suggest a straightforward strategy for mesh adaptivity which is demonstrated on numerical hyperbolic problems of interest.

Key words: *A posteriori* error estimates, error representation, Godunov finite volume methods, finite element methods, unstructured meshes.

1.1 Introduction

In the numerical simulation of partial differential equations, a frequently encountered objective in these simulations is the subsequent calculation of certain derived quantities of particular interest, e.g., aerodynamic lift and drag coefficients, stress intensity factors, mean temperatures, etc. The ability to estimate the error in such derived quantities (mathematically described as functionals) and modify the calculation procedure via adaptivity to efficiently decrease this error provides a systematic approach to improved reliability and efficiency of numerical simulations.

For an introduction to *a posteriori* error analysis of functionals see the articles by Becker and Rannacher [BR98], Eriksson et al. [EEHJ95], Giles et al. [GLLS97, GP99], Johnson et al. [JRB95], Prudhomme and Oden [OP99, PO99], Süli [S̈98], the collected NATO lecture notes [BD02] and the multitude of additional references contained therein. The main goal of this work is to provide a brief introduction to these general theories for nonlinear conservation laws and to relate specialized theories for the Godunov finite volume method as described in Barth and Larson [BL02] and the discontinuous Galerkin method as described in Larson and Barth [LB99] as well as Hartmann and Houston [HH02]. Comparison of these theories exposes important differences between finite element and finite volume methods with respect to the error representation of functionals. This is due to the absence of full Galerkin orthogonality in Godunov finite volume methods, namely that element (cell) residuals in the finite element method are orthogonal to a much larger space of functions than are residuals in the finite volume method. Consequently, finite element and finite volume methods with identical rates of convergence for global error measures can have dramatically different rates of convergence for derived functionals. Another consequence is that the dual (adjoint) problem used in the error representation formula for functionals can be approximated in Godunov finite volume methods using the same order method (same space of reconstructed functions) as used in the primal problem. Attempting this same strategy using the finite element methods considered herein fails completely since by Galerkin orthogonality the estimated error is identically zero. For the finite element method, the dual problem must be approximated in a larger space of functions than used in the primal numerical method.

1.2 Background

Consider the following system of m first-order conservation laws in a domain $\Omega \subset \mathbf{R}^d$ with boundary Γ

$$\begin{cases} \sum_{i=1}^{d} f^i_{,x_i}(u) = 0 \ , & \text{for } x \text{ in } \Omega \\ A^-(g-u)|_\Gamma = 0 \ , & \text{for } x \text{ on } \Gamma \end{cases} \tag{1.1}$$

where $u(x) : \mathbf{R}^d \mapsto \mathbf{R}^m$ denotes the vector of conserved variables, $f^i(u) : \mathbf{R}^m \mapsto \mathbf{R}^m, i = 1, \ldots, d$ the flux vector components, and $A \equiv \sum_{i=1}^{d} n_i f^i_{,u}$ the flux jacobian matrix associated with a direction, n, normal to Γ. In the present discussion, only spatial derivatives are considered but more generally x could include a time coordinate without introducing any new complication in the abstract error representation formulas given below.

Let $\mathcal{K}$ be a partition of a polygonal domain Ω into non-overlapping shape regular elements (or control volumes) denoted by K. Furthermore, consider two finite-dimensional spaces of piecewise polynomials with differing degrees

of interelement continuity. The first space, $\mathcal{V}_{h,p}$, is the standard finite element space of piecewise polynomials of complete degree p with C^0 continuity between elements

$$\mathcal{V}_{h,p} = \{v \,:\, v \in C^0(\Omega), v|_K \in \mathcal{P}_p(K) \;,\; \forall K \in \mathcal{K}\} \tag{1.2}$$

with $\mathcal{P}_p(K)$ the space of polynomials of degree $\leq p$ defined on an element K. The second space, $\mathcal{V}^{\mathrm{B}}_{h,p}$, is the mesh dependent broken space of piecewise polynomials of complete degree p in each K with no continuity between elements

$$\mathcal{V}^{\mathrm{B}}_{h,p} = \{v \,:\, v|_K \in \mathcal{P}_p(K) \;,\; \forall K \in \mathcal{K}\} \;. \tag{1.3}$$

Using this latter broken space, two seemly different methods are considered. The first method is the the discontinuous Galerkin (DG) finite element method introduced by Reed and Hill [RH73] as analyzed by Johnson and Pitkäranta [JP86] and further refined for nonlinear conservation laws by Cockburn et al. [CLS89, CS97].

Discontinuous Galerkin FEM. Find $u_h \in \mathcal{V}^{\mathrm{B}}_{h,p}$ such that

$$\mathcal{B}_{\mathrm{DG}}(u_h, v) = F(v), \quad \forall v \in \mathcal{V}^{\mathrm{B}}_{h,p} \tag{1.4}$$

where

$$\begin{aligned}\mathcal{B}_{\mathrm{DG}}(u_h, v) - F(v) = \sum_{K\in\mathcal{K}} \Big(&- \int_K \sum_{i=1}^{d} v_{,x_i} \cdot f^i(u_h)\, dx \\ &+ \int_{\partial K \setminus \Gamma} v_- \cdot h(n; (u_h)_-, (u_h)_+)\, ds + \int_{\partial K \cap \Gamma} v_- \cdot h(n; (u_h)_-, g)\, ds \Big)\end{aligned} \tag{1.5}$$

where $h(n; u_-, u_+)$ is a numerical flux function such that $\sum_{i=1}^{d} n_i\, f^i(u) = h(n; u, u)$ and $h(n; u_-, u_+) = -h(-n; u_+, u_-)$.

The second method considered is the generalization of Godunov's original method [God59] to higher order accuracy via various forms of data reconstruction, e.g. MUSCL in [vL79], TVD in [Har83], UNO in [HOEC87], ENO in [Har89], and further generalization to unstructured meshes given in [BJ89, BF90, DOE90, Bar98, Abg94, Van93]. Recently, in Barth and Larson [BL02] the generalized Godunov finite volume method was shown equivalent to a particular Petrov-Galerkin variant of the discontinuous Galerkin method:

Higher Order Godunov FVM. Find $u_0 \in \mathcal{V}^{\mathrm{B}}_{h,0}$ such that

$$\mathcal{B}_{\mathrm{DG}}(R^0_p u_0, v) = F(v), \quad \forall v \in \mathcal{V}^{\mathrm{B}}_{h,0}, \quad R^0_p : \mathcal{V}^{\mathrm{B}}_{h,0} \mapsto \mathcal{V}^{\mathrm{B}}_{h,p} \tag{1.6}$$

where $\mathcal{B}_{\mathrm{DG}}$ is the same semilinear form used in the discontinuous Galerkin method and R^0_p is any patchwise reconstruction operator that maps the broken space of piecewise constants to the broken space of piecewise polynomials of complete degree p.

Using either of these methods, the objective is to estimate the error in a user specified functional $M(u)$ which can be expressed as a weighted integration over the domain Ω

$$M_\psi(u) = \int_\Omega \psi \cdot N(u)\, dx$$

or a weighted integration on the boundary Γ

$$M_\psi(u) = \int_\Gamma \psi \cdot N(u)\, dx$$

for some user specified weighting function $\psi(x) : \mathbf{R}^d \mapsto \mathbf{R}^m$ and linear/nonlinear function $N(u) : \mathbf{R}^m \mapsto \mathbf{R}^m$. By an appropriate choice of $\psi(x)$ and $N(u)$, it is possible to devise functionals of practical engineering use, e.g. lift and drag forces on a body, stress intensity factors, average quantities, etc.

In the remainder of this article, the connection between local error and nonlocal cell residuals is given. This is accomplished through the introduction of a dual (adjoint) problem. Error representation formulas using these dual problems are then constructed for the following quantities of interest:

- (Finite Element) $M_\Psi(u) - M_\Psi(u_h)$ where $u_h \in \mathcal{V}_{h,p}^{\mathrm{B}}$.
- (Godunov Finite Volume) $M_\Psi(u) - M_\Psi(R_p^0 u_0)$ with $u_0 \in \mathcal{V}_{h,0}^{\mathrm{B}}$ where $R_p^0 u_0$ is the reconstructed data in the Godunov finite volume method.

With error representation formulas in hand, superconvergence properties of certain functionals is briefly examined. This identifies some distinct differences between finite element and Godunov finite volume methods. The error representation formulas suggest simplified error estimates and a strategy for mesh adaptivity which is demonstrated on numerical problems of interest.

1.3 Error Representation for Hyperbolic Problems

In this section, the notion of local error representation for hyperbolic problems is revisited. Consider the primal scalar hyperbolic problem

$$\begin{cases} \mathcal{L}u = f & \text{for } x \text{ in } \Omega \\ u|_\Gamma = g & \text{for } x \text{ on } \Gamma^- \end{cases} . \tag{1.7}$$

For illustrative purposes, let $\mathcal{L}$ denote the advection operator

$$\mathcal{L}u \equiv \lambda \cdot \nabla u \tag{1.8}$$

with $\lambda(x) : \mathbf{R}^d \mapsto \mathbf{R}^d$. In this particular case, the inflow boundary is defined by

$$\Gamma^- = \{x \mid x \in \Gamma \text{ and } \lambda \cdot n < 0\} \tag{1.9}$$

with n the exterior normal vector on Γ. Next introduce the Green's function $G(\xi; x)$ satisfying adjoint problem

$$\begin{cases} \mathcal{L}^* G(\xi; x) = \delta(x - \xi) & \text{for } x \text{ in } \Omega \\ G(\xi; x)|_{\Gamma} = 0 & \text{for } x \text{ on } \Gamma^+ \end{cases} \tag{1.10}$$

where $\mathcal{L}^*$ is the adjoint operator and Γ^+ the outflow boundary, $\Gamma^+ \equiv \Gamma \setminus \Gamma^-$. The Green's function quantifies the connection between the *local* solution error and *nonlocal* residuals. Let $(u, v)_\Omega \equiv \int_\Omega u \cdot v \, dx$ and consider the solution error at a point $\xi \in \Omega$ for $u_h \in \mathcal{V}_{h,p}$

$$\begin{aligned} (u_h - u)(\xi) &= (u_h - u, \delta(x - \xi))_\Omega \\ &= (u_h - u, \mathcal{L}^* G(\xi; x))_\Omega \\ &= (\mathcal{L}(u_h - u), G(\xi; x))_\Omega \\ &= (R(u_h), G(\xi, x))_\Omega \end{aligned} \tag{1.11}$$

where $R(u_h) = \mathcal{L}u_h - f$ is the numerical residual. Absent from the final right-hand side equation is the exact solution u. This latter formula reveals the dependence of pointwise error on nonlocal numerical residuals. The error at a point ξ is a Green's function weighted combination of numerical residual errors integrated over the domain.

In the PDE system generalization, the associated Green's function components can become quite complicated (and counterintuitive) so that heuristic error estimation methods are more likely to fail. For example, Fig. 1.1 shows Green's function components for steady ideal magnetohydrodynamic flow with a velocity V and velocity aligned magnetic induction field B. Figure 1.1 (left) shows isodensity contours of the numerically computed Green's function for a uniform super Alfvén MHD flow indicating how numerical errors at a point in the center of the domain depend on local residual errors occurring in an *upstream* domain of dependence associated with the streamline and the fast magnetoacoustic characteristic cone. Decreasing the velocity magnitude while keeping the magnetic field fixed in this problem eventually gives rise to slow magnetoacoustic "forward inclined" waves (not found in hydrodynamics) so that now the same error components at a point in the center of the domain depend on residual errors occurring both *upstream* along the streamline and *downstream* along a cone associated with slow magnetoacoustic waves.

1.4 Error Representation Formulas for Functionals

In this section, exact error representation formulas are derived for three abstract formulations with
(1) $B_{\mathrm{DG}}(\cdot, \cdot)$ a bilinear form with $M(\cdot)$ a linear functional.
(2) $\mathcal{B}_{\mathrm{DG}}(\cdot, \cdot)$ a semilinear form (nonlinear in the first argument and linear in the second argument) with $\mathcal{M}(\cdot)$ a nonlinear functional.
(3) $\mathcal{B}_{\mathrm{DG}}(R_p^0 \cdot, \cdot)$ a semilinear form with $\mathcal{M}(\cdot)$ a nonlinear functional.

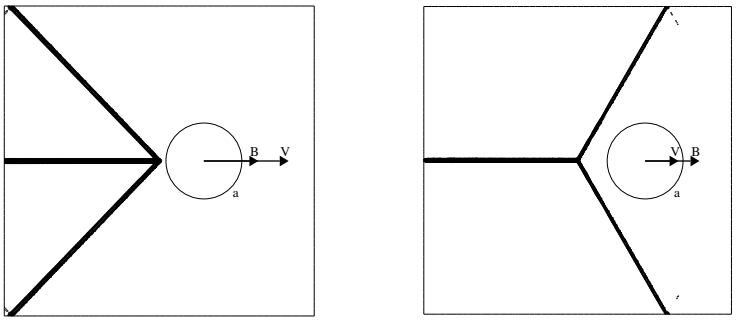

Fig. 1.1. Isocontours of the numerically computed Green's function density component for the 2-D steady ideal magnetohydrodynamic equations for a point ξ located at the center of the unit square domain. Streamline and fast magnetoacoustic wave front (left figure) corresponding to super Alfvén flow $|V|/c = 2, |B|/(c\sqrt{\rho}) = 1.2$. Streamline and slow magnetoacoustic forward inclined wave front (right figure), $|V|/c = .88, |B|/(c\sqrt{\rho}) = 1.2$.

Remark 1. To simplify the derivation of the error representation formulas, all boundary conditions are assumed weakly enforced rather than equipping the trial space with strong boundary condition data. This technique avoids the tedious explicit calculation of strong boundary conditions for the dual problem.

1.4.1 DG FEM Error Representation: The Linear Case

Let $B_{\mathrm{DG}}(\cdot,\cdot)$ denote a bilinear form and $M(\cdot)$ a linear functional. In the following derivations, π_h denotes any suitable projection operator (e.g. interpolation, L_2 projection) into $\mathcal{V}_{h,p}^{\mathrm{B}}$. Begin by introducing the primal numerical method assuming all boundary conditions are weakly enforced.

Primal numerical problem: *Find* $u_h \in \mathcal{V}_{h,p}^{\mathrm{B}}$ *such that*

$$B_{\mathrm{DG}}(u_h, v) = F(v) \quad \forall\ v \in \mathcal{V}_{h,p}^{\mathrm{B}}$$

with the Galerkin orthogonality condition

$$B_{\mathrm{DG}}(u - u_h, v) = 0 \quad \forall\ v \in \mathcal{V}_{h,p}^{\mathrm{B}}\ .$$

Next, we introduce the auxiliary dual problem utilizing infinite-dimensional trial and test spaces.

Dual problem: *Find* $\Phi \in \mathcal{V}^{\mathrm{B}}$ *such that*

$$B_{\mathrm{DG}}(v, \Phi) = M(v) \quad \forall\ v \in \mathcal{V}^{\mathrm{B}}\ .$$

An exact error representation formula for a given functional $M(\cdot)$ results from the following steps

$$\begin{aligned} M(u) - M(u_h) &= M(u - u_h) && \text{(linearity of } M\text{)} \\ &= B_{\mathrm{DG}}(u - u_h, \Phi) && \text{(dual problem)} \\ &= B_{\mathrm{DG}}(u - u_h, \Phi - \pi_h\Phi) && \text{(orthogonality)} \\ &= B_{\mathrm{DG}}(u, \Phi - \pi_h\Phi) - B_{\mathrm{DG}}(u_h, \Phi - \pi_h\Phi) && \text{(linearity of } B\text{)} \\ &= F(\Phi - \pi_h\Phi) - B_{\mathrm{DG}}(u_h, \Phi - \pi_h\Phi) && \text{(primal problem)} \end{aligned}$$

so in summary

$$M(u) - M(u_h) = F(\Phi - \pi_h\Phi) - B_{\mathrm{DG}}(u_h, \Phi - \pi_h\Phi) \ . \tag{1.12}$$

Notably absent from the right-hand side of this equation is any dependence on the exact solution u.

1.4.2 DG FEM Error Representation: The Nonlinear Case

Let $\mathcal{B}_{\mathrm{DG}}(\cdot,\cdot)$ denote a semilinear form and $\mathcal{M}(\cdot)$ a nonlinear functional. To cope with nonlinearity, mean-value linearization is employed

$$\begin{aligned} \mathcal{B}_{\mathrm{DG}}(u, v) &= \mathcal{B}_{\mathrm{DG}}(u_h, v) + \overline{\mathcal{B}}_{\mathrm{DG}}(u_h, u; u - u_h, v) \quad \forall\ v \in \mathcal{V}^{\mathrm{B}} \\ \mathcal{M}(u) &= \mathcal{M}(u_h) + \overline{\mathcal{M}}(u_h, u; u - u_h) \ . \end{aligned}$$

For example, if $\mathcal{B}(u, v) = (\mathcal{L}u, v)$ for some nonlinear differential operator $\mathcal{L}$ then for $v \in \mathcal{V}$

$$\begin{aligned} \mathcal{B}(u, v) &= \mathcal{B}(u_h, v) + \Big(\int_0^1 \mathcal{L}_{,u}(\tilde{u}(\theta))\, d\,\theta\ (u - u_h), v \Big) \\ &= \mathcal{B}(u_h, v) + (\overline{\mathcal{L}}_{,u}\,(u - u_h), v) \\ &= \mathcal{B}(u_h, v) + \overline{\mathcal{B}}(u_h, u; u - u_h, v). \end{aligned}$$

with $\tilde{u}(\theta) \equiv u_h + (u - u_h)\ \theta$. For brevity, the dependence of $\overline{\mathcal{B}}$ on the path integration involving the exact solution u will be notationally suppressed. We then proceed in the same fashion as in the previous example.

Primal numerical problem: *Find* $u_h \in \mathcal{V}^{\mathrm{B}}_{h,p}$ *such that*

$$\mathcal{B}_{\mathrm{DG}}(u_h, v) = F(v) \quad \forall\ v \in \mathcal{V}^{\mathrm{B}}_{h,p} \tag{1.13}$$

with orthogonality condition for the linearized form

$$\overline{\mathcal{B}}_{\mathrm{DG}}(u - u_h, v) = 0 \quad \forall\ v \in \mathcal{V}^{\mathrm{B}}_{h,p} \ .$$

A mean-value linearized dual problem is then introduced which utilizes infinite-dimensional trial and test spaces.

Linearized dual problem: *Find* $\Phi \in \mathcal{V}^{\mathrm{B}}$ *such that*

$$\overline{\mathcal{B}}_{\mathrm{DG}}(v, \Phi) = \overline{\mathcal{M}}(v) \quad \forall\ v \in \mathcal{V}^{\mathrm{B}} \ . \tag{1.14}$$

An exact error representation formula for a given nonlinear functional $\mathcal{M}(\cdot)$ then results from the following steps

$$\begin{aligned}
\mathcal{M}(u) - \mathcal{M}(u_h) &= \overline{\mathcal{M}}(u - u_h) && \text{(mean-value } \overline{\mathcal{M}}\text{)} \\
&= \overline{\mathcal{B}}_{\mathrm{DG}}(u - u_h, \Phi) && \text{(dual problem)} \\
&= \overline{\mathcal{B}}_{\mathrm{DG}}(u - u_h, \Phi - \pi_h\Phi) && \text{(orthogonality)} \\
&= \mathcal{B}_{\mathrm{DG}}(u, \Phi - \pi_h\Phi) - \mathcal{B}_{\mathrm{DG}}(u_h, \Phi - \pi_h\Phi) && \text{(mean-value } \overline{\mathcal{B}}\text{)} \\
&= F(\Phi - \pi_h\Phi) - \mathcal{B}_{\mathrm{DG}}(u_h, \Phi - \pi_h\Phi), && \text{(primal problem)}
\end{aligned}$$

so in summary

$$\mathcal{M}(u) - \mathcal{M}(u_h) = F(\Phi - \pi_h\Phi) - \mathcal{B}_{\mathrm{DG}}(u_h, \Phi - \pi_h\Phi) \ . \tag{1.15}$$

Note that although Eqns. (1.12) and (1.15) appear identical, mean-value linearization introduces a subtle right-hand side dependency on the exact solution in Eqn. (1.15).

1.4.3 Godunov FVM Error Representation

$\mathcal{B}_{\mathrm{DG}}(R_p^0\cdot, \cdot)$ and $\mathcal{M}(\cdot)$ are both assumed nonlinear. Mean-value linearizations are introduced as in the previous case

$$\begin{aligned}
\mathcal{B}_{\mathrm{DG}}(u, v) &= \mathcal{B}_{\mathrm{DG}}(R_p^0 u_0, v) + \overline{\mathcal{B}}_{\mathrm{DG}}(u - R_p^0 u_0, v) \quad \forall\ v \in \mathcal{V}^{\mathrm{B}} \\
\mathcal{M}(u) &= \mathcal{M}(R_p^0 u_0) + \overline{\mathcal{M}}(u - R_p^0 u_0)
\end{aligned}$$

for $u_0 \in \mathcal{V}_{h,0}^{\mathrm{B}}$ where the mean-value linearized forms again depend on a path integration involving the exact solution.

Primal Godunov FVM problem: *Find* $u_0 \in \mathcal{V}_{h,0}^{\mathrm{B}}$ *such that*

$$\mathcal{B}_{\mathrm{DG}}(R_p^0 u_0, v) = F(v) \quad \forall\ v \in \mathcal{V}_{h,0}^{\mathrm{B}} \tag{1.16}$$

with the orthogonality condition

$$\overline{\mathcal{B}}_{\mathrm{DG}}(u - R_p^0 u_0, v) = 0 \quad \forall\ v \in \mathcal{V}_{h,0}^{\mathrm{B}} \ .$$

Next, introduce the infinite-dimensional linearized dual problem.

Linearized dual problem: *Find* $\Phi \in \mathcal{V}^{\mathrm{B}}$ *such that*

$$\overline{\mathcal{B}}_{\mathrm{DG}}(v, \Phi) = \overline{\mathcal{M}}(v) \quad \forall\ v \in \mathcal{V}^{\mathrm{B}} \ . \tag{1.17}$$

An exact error representation formula for a given nonlinear functional $\mathcal{M}(\cdot)$ for the class of Godunov finite volume methods results from the following steps

$$\begin{aligned}
\mathcal{M}(u)-\mathcal{M}(R_p^0 u_0) &= \overline{\mathcal{M}}(u - R_p^0 u_0) && \text{(mean-value } \overline{\mathcal{M}}) \\
&= \overline{\mathcal{B}}_{\mathrm{DG}}(u - R_p^0 u_0, \Phi) && \text{(dual problem)} \\
&= \overline{\mathcal{B}}_{\mathrm{DG}}(u - R_p^0 u_0, \Phi - \pi_0\Phi) && \text{(orthogonality)} \\
&= \mathcal{B}_{\mathrm{DG}}(u, \Phi - \pi_0\Phi) - \mathcal{B}_{\mathrm{DG}}(R_p^0 u_0, \Phi - \pi_0\Phi) && \text{(mean-value } \overline{\mathcal{B}}) \\
&= F(\Phi - \pi_0\Phi) - \mathcal{B}_{\mathrm{DG}}(R_p^0 u_0, \Phi - \pi_0\Phi), && \text{(primal problem)}
\end{aligned}$$

with π_0 any projection into $\mathcal{V}_{h,0}$ thus yielding the following exact error representation formula

$$\mathcal{M}(u) - \mathcal{M}(R_p^0 u_0) = F(\Phi - \pi_0\Phi) - \mathcal{B}_{\mathrm{DG}}(R_p^0 u_0, \Phi - \pi_0\Phi) \ . \tag{1.18}$$

Again, it should be noted that the right-hand side has a subtle dependence on the exact solution through the mean-value linearization used in the dual problem.

1.4.4 Superconvergence of Functionals

In this section, convergence rates for functionals is examined. Recall the error representation formulas for the discontinuous Galerkin and Godunov finite volume methods.

Discontinuous Galerkin Finite Element

$$\mathcal{M}(u) - \mathcal{M}(u_h) = F(\Phi - \pi_h\Phi) - \mathcal{B}_{\mathrm{DG}}(u_h, \Phi - \pi_h\Phi) \tag{1.19}$$

Godunov Finite Volume Method

$$\mathcal{M}(u) - \mathcal{M}(R_p^0 u_0) = F(\Phi - \pi_0\Phi) - \mathcal{B}_{\mathrm{DG}}(R_p^0 u_0, \Phi - \pi_0\Phi) \ . \tag{1.20}$$

A notable difference between the discontinuous Galerkin method and the Godunov finite volume method comes from the orthogonality condition used in the derivation of the error representation formulas. In the finite element method, the error $u - u_h$ is Galerkin orthogonal to all test functions in $\mathcal{V}_{h,p}$ with respect to the bilinear form $\overline{\mathcal{B}}_{\mathrm{DG}}(\cdot,\cdot)$. In the finite volume method, the error $u - R_p^0 u_0$ is only orthogonal to constant test functions with respect to the same bilinear form. So even if the convergence rates for global error measures using the finite volume and finite element methods are the same, the convergence rates for functionals can be quite different. In the setting of linear advection-diffusion problems, the superconvergence theory for functionals is understood. For example, Süli and Houston in [BD02] give the convergence theory of functionals for the streamline diffusion discretization of scalar hyperbolic problems. For problems with sufficiently smooth primal and dual solutions, the basic theoretical result for streamline diffusion states that if the primal method converges at the rate $\mathcal{O}(h^{p+1/2})$ then functionals converge at

the rate $\mathcal{O}(h^{2p+1})$. When diffusion terms are added to the PDE the convergence rate of functionals becomes $\mathcal{O}(h^{2p})$.

The analysis of functionals for the discontinuous Galerkin method is a trivial extension of the streamline diffusion analysis. Consider the scalar advection problem given in (1.7-1.8). The well-known *a priori* theory [JP86, Joh87] for the discontinuous Galerkin method (with interior stabilization added only for theoretical analysis purposes) gives the following convergence result

$$|||u - u_h|||^2 \leq h^{2s+1}|u|^2_{H^{s+1}(\Omega)}$$

where

$$|||v||| = \sum_{K\in\mathcal{K}} \left(h\|\mathcal{L}v\|^2_K + \|v\|^2_{\partial K^-\cap\Gamma^-} + \frac{1}{2}\|v\|^2_{\partial K^+\cap\Gamma^+} + \frac{1}{2}\|[v]^+_-\|^2_{\partial K^-\setminus\Gamma} \right)$$

for $0 \leq s \leq p$. The discontinuous Galerkin method for (1.7-1.8) then reduces to the following problem:

Find $u_h \in \mathcal{V}^B_{h,p}$ *such that* $\forall v \in \mathcal{V}_{h,p}$

$$\sum_{K\in\mathcal{K}} (\mathcal{L}u_h - f, v + \delta_h\mathcal{L}v)_K + \langle (\lambda\cdot n)^- [u]^+_-, v_-\rangle_{\partial K\setminus\Gamma} + \langle (\lambda\cdot n)^- (g-u), v_-\rangle_{\partial K\cap\Gamma} = 0$$

where δ_h is $\mathcal{O}(h)$. Using the *a priori* theory for the discontinuous Galerkin method together with standard approximation theory, terms in the error representation formula are readily estimated

$$|M(u_h) - M(u)|_{\mathrm{DG}} = \mathrm{I} + \mathrm{II} + \mathrm{III} + \mathrm{IV}$$

with

$$\begin{aligned}
\mathrm{I} &= |\sum_{K\in\mathcal{K}} (\mathcal{L}u_h - f, \Phi - \pi_h\Phi)_K| \leq Ch^s|u|_{H^{s+1}(\Omega)}\times h^{s+1}|\Phi|_{H^{s+1}(\Omega)} \\
\mathrm{II} &= |\sum_{K\in\mathcal{K}} (\mathcal{L}u_h - f, \delta_h\mathcal{L}(\Phi - \pi_h\Phi))_K| \leq Ch^s|u|_{H^{s+1}(\Omega)}\times h^{s+1}|\Phi|_{H^{s+1}(\Omega)} \\
\mathrm{III} &= |\sum_{K\in\mathcal{K}} \langle (\lambda\cdot n)^- [u]^+_-, \Phi - \pi_h\Phi\rangle_{\partial K\setminus\Gamma} \leq Ch^{s+\frac{1}{2}}|u|_{H^{p+1}(\Omega)}\times h^{s+\frac{1}{2}}|\Phi|_{H^{s+1}(\Omega)} \\
\mathrm{IV} &= |\sum_{K\in\mathcal{K}} \langle (\lambda\cdot n)^-(g-u), \Phi - \pi_h\Phi\rangle_{\partial K\cap\Gamma} \leq Ch^{s+\frac{1}{2}}|u|_{H^{s+1}(\Omega)}\times h^{s+1}|\Phi|_{H^{s+1}(\Gamma^-)}
\end{aligned} \tag{1.21}$$

for $0 \leq s \leq p$. In these estimates, each right-hand side term has been written as the product of two estimates coming from the primal and dual data respectively. If the infinite-dimensional primal and dual solution data are sufficiently smooth so that $|u|_{H^{p+1}(\Omega)}$ and $|\Phi|_{H^{p+1}(\Omega)}$ are bounded by a constant then

$$|M(u_h) - M(u)|_{\mathrm{DG}} \leq C\, h^{2p+1} \quad .$$

Examination of the right-hand side terms in (1.21) shows the important role of Galerkin orthogonality in attaining the "order doubling" superconvergence property of functionals in the discontinuous Galerkin method. Unfortunately, similar *a priori* results are not available for the Godunov finite volume method. If one only assumes orthogonality with respect to constants in the discontinuous Galerkin method then one would conclude from the above analysis that no superconvergence of functionals is attained. Fortunately, the computations given next indicate that this is not the case in the Godunov method and some limited superconvergence is observed but the prospect of order doubling is lost.

Method	dofs	h	p	Global Error $\|u-u_h\|_{L^2}$ (rate)	Functional Error $\|M(u)-M(\tilde{u}_h)\|$ (rate)
DG FEM	1200	.0616	1	.639e-2	.232e-3
DG FEM	4800	.0258	1	.171e-2 (1.51)	.168e-4 (3.02)
DG FEM	19200	.0134	1	.390e-3 (2.26)	.217e-5 (3.12)
DG FEM	76800	.0071	1	.992e-4 (2.16)	.275e-6 (3.25)
Godunov FV	1600	.0258	1	.365e-2	.136e-3
Godunov FV	6400	.0134	1	.836e-3 (2.25)	.169e-4 (3.20)
Godunov FV	25600	.0071	1	.167e-3 (2.36)	.214e-5 (3.25)
Godunov FV	102400	.0036	1	.416e-4 (2.21)	.262e-6 (3.09)
DG FEM	2400	.0616	2	.936e-3	.128e-5
DG FEM	9600	.0258	2	.977e-4 (2.60)	.247e-7 (4.54)
DG FEM	38400	.0138	2	.108e-4 (3.51)	.110e-8 (4.97)
DG FEM	153600	.0071	2	.132e-5 (3.16)	.374e-10 (5.09)
Godunov FV	1600	.0258	2	.278e-2	.882e-4
Godunov FV	6400	.0134	2	.522e-3 (2.55)	.874e-5 (3.52)
Godunov FV	25600	.0071	2	.855e-3 (2.84)	.884e-6 (3.60)
Godunov FV	102400	.0036	2	.135e-4 (2.72)	.980e-7 (3.24)

Table 1.1. Convergence characteristics of the DG finite element and Godunov finite volume methods for the circular advection problem (1.22). Tabulated data for the global $L^2(\Omega)$ error and error in the weighted outflow flux functional.

To numerically verify the convergence rate of functionals for smooth primal and dual data, numerical solutions of the following 2-D advection problem were obtained using the discontinuous Galerkin finite element method and the Godunov finite volume method with least-squares reconstruction operator as described in Barth and Larson [BL02]:

$$\begin{cases} \lambda \cdot \nabla u = \quad 0 \quad \text{for } (x,y) \in [0,1]^2 \ , \\ u(1,y) = g_1(y) \ , \\ u(x,0) = g_2(x) \ , \end{cases} \tag{1.22}$$

with circular advection field $\lambda = (-y,x)^T$, $g_1(y) = 0$, and

$$g_2(x) = \begin{cases} \widetilde{\psi}(9/20; |x - 1/2|) \cdot (1 - \widetilde{\psi}(9/20; |x - 1/20|)) & \text{if } x \le 1/2 \\ \widetilde{\psi}(9/20; |x - 1/2|) \cdot (1 - \widetilde{\psi}(9/20; |x - 19/20|)) & \text{if } x > 1/2 \end{cases}$$

where $\widetilde{\psi}(\cdot;\cdot)$ is a C^∞ function

$$\widetilde{\psi}(r_0; r) = \begin{cases} 0 & r \ge r_0 \\ e^{1 + r_0^2/(r^2 - r_0^2)} & r < r_0 \end{cases} . \tag{1.23}$$

In addition, the weighted outflow flux functional

$$M_\psi(u) = \int_0^1 \psi_{\text{outflow}}(y)\, (\lambda \cdot n)^+ u(0, y)\, dy \tag{1.24}$$

was computed using the weighting function

$$\psi_{\text{outflow}}(y) = \begin{cases} \widetilde{\psi}(7/20; |y - 3/5|) \cdot (1 - \widetilde{\psi}(7/20; |y - 1/4|)) & \text{if } y \le 3/5 \\ \widetilde{\psi}(7/20; |y - 3/5|) \cdot (1 - \widetilde{\psi}(7/20; |y - 19/20|)) & \text{if } y > 3/5 \end{cases} . \tag{1.25}$$

This particular weighting function was chosen so that the corresponding dual solution would be smooth although the dual solution was not needed for the calculation of the functional error. Table 1.1 tabulates values of the global solution error and the error in the weighted outflow flux functional using a sequence of four meshes. The results using $p = 1$ approximation are very comparable between the finite element and finite volume methods. Each method shows second order convergence in the global L^2 error norm and third order convergence in the functional error. The numerical results using $p = 2$ approximation for the discontinuous Galerkin method confirm or exceed the theoretically estimated rates for both the global L^2 error (third order) and the error in the weighted outflow functional (fifth order). Less favorably, the results for the Godunov finite volume method with $p = 2$ approximation show an improvement of no more than one power of h in the convergence rate of functional error when compared to the convergence rate of the global L^2 error. Although the numerical results for the Godunov finite volume method are far from conclusive and may depend on the details of the reconstruction operator, the results do indicate a marked difference between the finite element and finite volume method when computing functionals. It is conjectured that this difference can be explained to some extent by the lack of full Galerkin orthogonality in the finite volume method. Further analysis beyond the scope of this article is clearly needed to more fully explain the performance of the Godunov finite volume method.

1.5 Computable Error Estimates and Adaptivity

Computationally, the error representation formulas (1.12), (1.15) and (1.18) are not suitable for obtaining computable *a posteriori* error estimates and use in mesh adaptation.

- The functions $\Phi - \pi_h\Phi$ and $\Phi - \pi_0\Phi$ are unknown where $\Phi \in \mathcal{V}^B$ is a solution of the infinite-dimensional dual problem.
- The mean-value linearization used in the linearized dual problems (1.14) and (1.17) requires knowledge of the exact solution u.

Various strategies which address the numerical approximation of Φ are discussed in Barth and Larson [BL02], e.g. postprocessing, higher order solves, etc. Due to Galerkin orthogonality, the dual problem in the discontinuous Galerkin finite element method must be approximated in a larger space of functions than that utilized in the primal numerical problem. For purposes of the present study, this is achieved in the discontinuous Galerkin method by solving the dual problem using a polynomial space that is one polynomial degree higher than the primal numerical problem, viz. if $u_h \in \mathcal{V}^{\mathrm{B}}_{h,p}$ then $\Phi \approx \Phi_h \in \mathcal{V}^{\mathrm{B}}_{h,p+1}$. For the Godunov finite volume method, π_0 is the projection to piecewise constants. Consequently, the dual problem can be approximated using the same reconstruction operator as used in the primal problem ($p \neq 0$). In practice, there may be some additional improvement in accuracy by using an even higher order method for numerically approximating the dual problem. This is experimentally considered in Sect. 1.6.

In the present study, the mean-value linearization depending on the states u and u_h is replaced by the simpler jacobian linearization evaluated at the numerical state u_h. This is not the only practical choice. In Barth and Larson [BL02], a more sophisticated technique involving the postprocessing of primal data and the approximation of the mean-value linearization by numerical quadrature is employed in computations.

1.5.1 Direct Estimates

For brevity, the error representation formulas for the discontinuous Galerkin and Godunov finite volume methods can be combined into a single formula

$$\mathcal{M}(u) - \mathcal{M}(\tilde{u}_h) = F(\Phi - \pi\Phi) - \mathcal{B}_{\mathrm{DG}}(\tilde{u}_h, \Phi - \pi\Phi) \tag{1.26}$$

where $\tilde{u}_h \equiv u_h$, $\pi \equiv \pi_h$ for the discontinuous Galerkin method and $\tilde{u}_h \equiv R^0_p u_0$, $\pi \equiv \pi_0$ for the Godunov finite volume method. When written in this global abstract form, the error representation formula does not indicate which elements in the mesh should be refined to reduce the measured error in a functional. By applying a sequence of direct estimates, error bounds suitable for adaptive meshing are easily obtained. The goal in constructing these estimates is to estimate the *local* contribution of each element in the mesh to the functional error. This local cell contribution will then be used as an error indicator for choosing which elements to refine or coarsen in the adaptive mesh procedure.

$$
\begin{aligned}
|\mathcal{M}(u) - \mathcal{M}(\tilde{u}_h)| &= |\mathcal{B}_{\mathrm{DG}}(\tilde{u}_h, \Phi - \pi\Phi) - F(\Phi - \pi\Phi)| \quad \text{(error representation)} \\
&= |\sum_{K\in\mathcal{K}} \big(\mathcal{B}_{\mathrm{DG},K}(\tilde{u}_h, \Phi - \pi\Phi) - F_K(\Phi - \pi\Phi)\big)| \quad \text{(element assembly)} \\
&\le \sum_{K\in\mathcal{K}} \big|\big(\mathcal{B}_{\mathrm{DG},K}(\tilde{u}_h, \Phi - \pi\Phi) - F_K(\Phi - \pi\Phi)\big)\big| \quad \text{(triangle inequality)}
\end{aligned}
\tag{1.27}
$$

where $\mathcal{B}_{\mathrm{DG},K}(\cdot,\cdot)$ and $F_K(\cdot)$ are restrictions of $\mathcal{B}_{\mathrm{DG}}(\cdot,\cdot)$ and $F(\cdot)$ to the partition element K. The basic definition of the discontinuous Galerkin semilinear form given in (1.5) shows one possible element assembly form but this is not a unique representation. For example strong and weak forms of the semilinear operator $\mathcal{B}_{\mathrm{DG}}(\cdot,\cdot)$ yield differing assembly representations. For the discontinuous Galerkin and Godunov finite volume methods, the error representation formula (1.26) together with (1.5) for a single element K yields

$$
\begin{aligned}
\mathcal{B}_{\mathrm{DG},K}(\tilde{u}_h, \Phi - \pi\Phi) - F_K(\Phi - \pi\Phi) = &- \int_K \sum_{i=1}^{d} f^i(\tilde{u}_h)\cdot(\Phi - \pi\Phi)_{,x_i}\, dx \\
&+ \int_{\partial K\setminus\Gamma} (\Phi - \pi\Phi)_- \cdot h(n; (\tilde{u}_h)_-, (\tilde{u}_h)_+)\, ds \\
&+ \int_{\partial K\cap\Gamma} (\Phi - \pi\Phi)_- \cdot h(n; (\tilde{u}_h)_-, g)\, ds\Big) \ .
\end{aligned}
\tag{1.28}
$$

The present numerical computations utilize the numerical flux formula

$$
h(n; u_-, u_+) = \frac{1}{2}\left(f(n; u_-) + f(n; u_+)\right) - \frac{1}{2}|A(n; \overline{u}(u_-, u_+))|\,[u]_-^+ \tag{1.29}
$$

with $f(n;u) = \sum_{i=1}^{d} n_i\, f^i(u_-)$ and $A(n;u) = \partial f(n;u)/\partial u$. The state $\overline{u}(u_-, u_+)$ is chosen so that

$$
[f(n;u)]_-^+ = A(n; \overline{u}(u_-, u_+))\,[u]_-^+ \ . \tag{1.30}
$$

Using this particular numerical flux, the following weighted residual (strong) form can be obtained upon integration by parts

$$
\begin{aligned}
\mathcal{B}_{\mathrm{DG},K}(\tilde{u}_h, \Phi - \pi\Phi) \,-\, F_K(\Phi - \pi\Phi) = &\int_K (\Phi - \pi\Phi)\cdot \sum_{i=1}^{d} f^i_{,x_i}(\tilde{u}_h)\, dx \\
&+ \int_{\partial K\setminus\Gamma} (\Phi - \pi\Phi)_- \cdot A^-(n; (\tilde{u}_h)_-, (\tilde{u}_h)_+)\,[\tilde{u}_h]_-^+\, ds \\
&+ \int_{\partial K\cap\Gamma} (\Phi - \pi\Phi)_- \cdot A^-(n; (\tilde{u}_h)_-, g)\,(g - (\tilde{u}_h)_-)\, ds\Big) \ .
\end{aligned}
\tag{1.31}
$$

This latter weighted residual form and the implied element assembly form $\sum_K \mathcal{B}_K(\cdot,\cdot) - F_K(\cdot)$ is preferred in the error estimates (1.27) since the individual terms represent residual components that vanish individually when

the exact solution is inserted into the variational form and a slightly sharper approximation is obtained after application of the triangle inequality in (1.27).

1.5.2 Adaptive Meshing

Motivated by the direct estimates (1.27), we define for each partition element K the *adaptation element indicator* $|\eta_K|$

$$\eta_K \equiv \mathcal{B}_{\mathrm{DG,K}}(\tilde{u}_h, \Phi - \pi\Phi) - F_K(\Phi - \pi\Phi) \ , \tag{1.32}$$

such that

$$|\mathcal{M}(u) - \mathcal{M}(\tilde{u}_h)| \leq \sum_{K\in\mathcal{K}} |\eta_K| \tag{1.33}$$

and an accurate *adaptation stopping criteria*

$$|\mathcal{M}(u) - \mathcal{M}(\tilde{u}_h)| = |\sum_{K\in\mathcal{K}} \eta_K| \ . \tag{1.34}$$

These quantities suggest a simple mesh adaptation strategy in common use with other indicator functions:

Mesh Adaptation Algorithm
(1) Construct an initial mesh $\mathcal{K}$.
(2) Compute a numerical approximation of the primal problem on the current mesh $\mathcal{K}$.
(3) Compute a suitable numerical approximation of the infinite-dimensional dual problem on the current mesh $\mathcal{K}$.
(4) Compute error indicators, η_K, for all elements $K \in \mathcal{K}$.
(5) If($|\sum_{K\in\mathcal{K}} \eta_K| < TOL$) STOP
(6) Otherwise, refine and coarsen a specified fraction of the total number of elements according to the size of $|\eta|_K$, generate a new mesh $\mathcal{K}$, and GOTO 2

1.6 Numerical Results

In this section, selected numerical examples are given for scalar advection and systems of nonlinear conservation laws. Further numerical examples can be found in [LB99] and [BL02].

1.6.1 Linear Advection

To assess the sharpness of the computable error estimates, the circular advection problem given in (1.22) is again considered. Table 1.2 tabulates values of the functional error and the estimated error as given in (1.27) using numerically approximated dual problems (see Sect. 1.5). In addition, the effectivity index is included to characterize sharpness of the estimates

Method	dofs	h	primal p	dual p	$\lvert M(u)-M(\tilde{u}_h)\rvert$	$\lvert\sum_K \eta_K\rvert$ (θ_{eff})	$\sum_K \lvert\eta_K\rvert$ (θ_{eff})
DG FEM	1200	.0616	1	2	.232e-3	.233e-3 (1.00)	.377e-3 (1.62)
DG FEM	4800	.0258	1	2	.168e-4	.168e-4 (1.00)	.380e-4 (2.26)
DG FEM	19200	.0134	1	2	.217e-5	.217e-5 (1.00)	.498e-5 (2.29)
DG FEM	76800	.0071	1	2	.275e-6	.276e-6 (1.00)	.582e-6 (2.11)
Godunov FV	1600	.0258	1	1	.136e-3	.100e-3 (.735)	.727e-3 (5.35)
Godunov FV	6400	.0134	1	1	.169e-4	.152e-4 (.900)	.167e-3 (9.88)
Godunov FV	25600	.0071	1	1	.214e-5	.188e-5 (.879)	.378e-4 (17.7
Godunov FV	102400	.0036	1	1	.262e-6	.245e-6 (.935)	.900e-5 (34.4)
Godunov FV	1600	.0258	1	2	.136e-3	.141e-3 (1.04)	.756e-3 (5.56)
Godunov FV	6400	.0134	1	2	.169e-4	.174e-4 (1.03)	.167e-3 (9.88)
Godunov FV	25600	.0071	1	2	.214e-5	.216e-5 (1.01)	.378e-4 (17.7)
Godunov FV	102400	.0036	1	2	.262e-6	.263e-6 (1.00)	.892e-5 (34.0)
DG FEM	2400	.0616	2	3	.128e-5	.959e-6 (.750)	.990e-5 (7.73)
DG FEM	9600	.0258	2	3	.247e-7	.237e-7 (.960)	.158e-6 (6.40)
DG FEM	38400	.0138	2	3	.110e-8	.109e-8 (.991)	.465e-8 (4.22)
DG FEM	153600	.0071	2	3	.374e-10	.373e-10 (.997)	.143e-9 (3.83)
Godunov FV	1600	.0258	2	2	.882e-4	.893e-4 (1.01)	.294e-3 (3.33)
Godunov FV	6400	.0134	2	2	.874e-5	.875e-5 (1.00)	.355e-4 (4.06)
Godunov FV	25600	.0071	2	2	.884e-6	.885e-6 (1.00)	.400e-5 (4.52)
Godunov FV	102400	.0036	2	2	.980e-7	.980e-7 (1.00)	.494e-6 (5.04)

Table 1.2. Efficiency of the DG finite element and Godunov finite volume methods error estimates for the circular advection problem (1.22). Tabulated data for the weighted outflow flux functional error and the estimates given in (1.27) .

$$\theta_{\text{eff}} \equiv \frac{|\text{estimated error}|}{|M(u) - M(\tilde{u}_h)|} \ .$$

Recall that when the exact dual solution Φ is used

$$|\mathcal{M}(u) - \mathcal{M}(\tilde{u}_h)| = |\sum_{K\in\mathcal{K}} \eta_K| \ .$$

Consequently, the seventh column measures the effect of numerically approximating the dual problem. For this particular test problem, the technique of approximating the dual problem using a higher order method for the discontinuous Galerkin method yields extremely accurate estimates of the functional error with θ_{eff} very close to unity. This comes at a fairly high price given the dramatic increase in arithmetic complexity of the discontinuous Galerkin method with increasing p. The results for the Godunov finite volume method show that reasonable estimates can be obtained by computing the dual problem with the same order method as the primal problem. For $p = 1$, some improvement in the Godunov finite volume method is achieved using a higher order method for the dual problem. For $p = 2$, the need for solving the dual problem using a higher order method seems entirely unnecessary since effectivity indices near unity are achieved.

After application of the triangle inequality, the estimate

$$|\mathcal{M}(u) - \mathcal{M}(\tilde{u}_h)| \leq \sum_{K \in \mathcal{K}} |\eta_K| \tag{1.35}$$

is obtained for use in mesh adaptivity. Column eight in Table 1.2 shows some loss in sharpness in this error estimate since the possibility of interelement error cancellation is precluded. Even so, the working assumption is that this estimate is sufficiently accurate to drive efficient mesh adaptivity. The results for the Godunov method with $p = 1$ for the primal numerical problem show no significant differences in the (1.35) estimate using either $p = 1$ or $p = 2$ solves for the dual problem. These numerical results again illustrate significant differences between the Godunov finite volume method and the discontinuous Galerkin methods that are worth further investigation.

1.6.2 Compressible Euler Flow

In this example, Ringleb flow (an exact solution of the 2-D Euler equations obtained via hodograph transformation, see [Chi85]) is computed in the channel geometry using the discontinuous Galerkin method with linear elements. To illustrate the use of the element indicators (1.32) in adaptive meshing, the mollified pointwise functional

$$M_\delta(u) = \int_\Omega \text{Energy}(u)\, \tilde{\psi}(r_0; |x - x_0|)\, dx \;\;, \quad x_0 = (-.63, 1.70)^T \;\;, \quad r_0 = 1/10$$

has been implemented for the energy component of the solution. Using this functional, the corresponding dual problem has been computed and the mesh adapted using the adaptation algorithm of Sect. 1.5.2. Figure 1.2 shows the resulting dual solution and the adapted mesh with three levels of refinement. The adapted mesh shows the upstream dependence of numerical residual er-

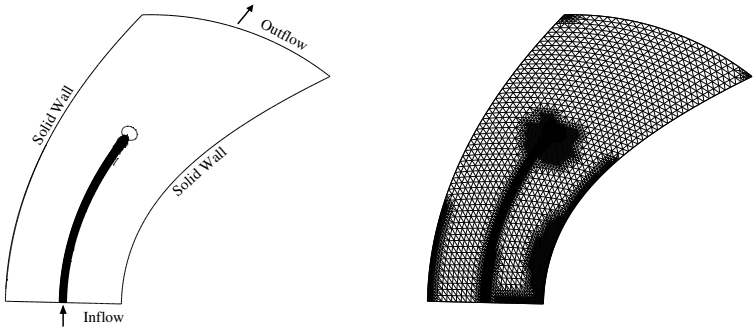

Fig. 1.2. Ringleb channel geometry. Dual energy isocontours solution corresponding to mollified delta functional (left) and final adapted mesh (3 levels) (right).

rors on the accuracy of this local functional. Further details of the mesh adaptation process are given in Table 1.3. This table also gives the approximate

Level	$\lvert M(u)-M(\tilde{u}_h)\rvert$	(Adaptive) # Mesh Cells	(Uniform) # Mesh Cells
0	2.40e-7	1482	1482
1	6.18e-8	2020	3422
2	8.82e-9	4010	14042
3	1.25e-9	10214	56882

Table 1.3. Performance of adaptive meshing algorithm for the Ringleb flow problem and the mollified pointwise energy functional.

number of cells needed in a uniformly refined mesh to achieve the same level of accuracy in the target functional. With just three levels of refinement, the number of mesh cells in the adapted mesh is reduced by over a factor of five from uniform refinement. This indicates the significant savings achieved by the adaptive algorithm.

1.7 Concluding Remarks

A simple *a posteriori* error estimation theory for user specified functionals has been constructed that is tailored to Godunov finite volume and discontinuous Galerkin methods. Many issues remain unresolved:

- Mean-value linearization for schemes with non-differentiable limiters and/or reconstruction algorithms.
- Existence and solvability of dual problems.
- Numerical approximation of dual problems.

Even though error representations formula have been developed for both linear and nonlinear functionals, very little is theoretically known about the existence or solvability of dual solutions for general functionals. The analysis is made particularly difficult since the linearized infinite-dimensional dual problem can have discontinuous coefficients. In practice, one often finds that dual solutions are more complicated in structure than the sought after primal solution. As an example, consider transonic Euler flow ($M\infty = .85, \alpha = 2.0^\circ$) over the NACA 0012 airfoil geometry. Suppose the aerodynamic lift functional is chosen for evaluation:

$$M_{\text{Lift}}(u) = \int_{\Gamma_{wall}} (n \cdot V^{\perp}/|V|)\,\text{Pressure}(u)\; d\,x \;\; .$$

Figure 1.3 shows isodensity contours of the primal solution and isodensity contours of the dual solution corresponding to the lift functional. The dual solution has a complicated structure with a large dipole singularity at the trailing edge of the airfoil and numerous layers emanating from the airfoil surface near the leading edge stagnation point, upper and lower sonic points, and the base of the upper and lower shockwaves. These structures signify the sensitivity of the lift force to these features. These structures place additional

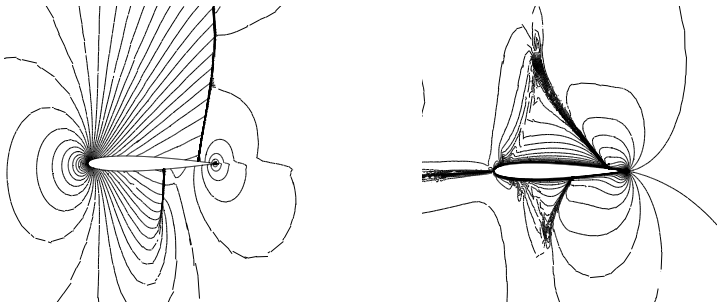

Fig. 1.3. NACA airfoil geometry, $M_\infty = .85, \alpha = 2.0^\circ$. Isodensity contours of primal solution (left) and corresponding contours of the dual density solution (right) for the lift functional.

demands on the discretization and suggests that the extension to 3-D is a truly challenging problem. This will be pursued in future work.

References

[Abg94] R. Abgrall. An essentially non-oscillatory reconstruction procedure on finite-element type meshes. *Comp. Meth. Appl. Mech. Engrg.*, 116:95–101, 1994.

[Bar98] T.J. Barth. Numerical methods for gasdynamic systems on unstructured meshes. In Kröner, Ohlberger, and Rohde, editors, *An Introduction to Recent Developments in Theory and Numerics for Conservation Laws*, volume 5 of *Lecture Notes in Computational Science and Engineering*, pages 195–285. Springer-Verlag, Heidelberg, 1998.

[BD02] T.J. Barth and H. Deconinck(eds). Error estimation and adaptive discretization methods in CFD. In Barth and Deconinck, editors, *Error Estimation and Adaptive Discretization Methods in CFD*, volume 25 of *Lecture Notes in Computational Science and Engineering*. Springer-Verlag, Heidelberg, 2002.

[BF90] T. J. Barth and P.O. Frederickson. Higher order solution of the Euler equations on unstructured grids using quadratic reconstruction. Technical Report 90-0013, AIAA, Reno, NV, 1990.

[BJ89] T. J. Barth and D. C. Jespersen. The design and application of upwind schemes on unstructured meshes. Technical Report 89-0366, AIAA, Reno, NV, 1989.

[BL02] T.J. Barth and M.G. Larson. A-posteriori error estimation for higher order Godunov finite volume methods on unstructured meshes. In Herbin and Kröner, editors, *Finite Volumes for Complex Applications III*, pages 41–63. Hermes Science Pub., London, 2002.

[BR98] R. Becker and R. Rannacher. Weighted a posteriori error control in FE methods. In *Proc. ENUMATH-97, Heidelberg*. World Scientific Pub., Singapore, 1998.

[Chi85] G. Chiocchia. Exact solutions to transonic and supersonic flows. Technical Report AR-211, AGARD, 1985.

[CLS89] B. Cockburn, S.Y. Lin, and C.W. Shu. TVB Runge-Kutta local projection discontinuous Galerkin finite element method for conservation laws III: One dimensional systems. *J. Comp. Phys.*, 84:90–113, 1989.

[CS97] B. Cockburn and C.W. Shu. The Runge-Kutta discontinuous Galerkin method for conservation laws V: Multidimensional systems. Technical Report 201737, Institite for Computer Applications in Science and Engineering (ICASE), NASA Langley R.C., 1997.

[DOE90] L. Durlofsky, S. Osher, and B. Engquist. Triangle based TVD schemes for hyperbolic conservation laws. Technical Report 90-10, Institite for Computer Applications in Science and Engineering (ICASE), NASA Langley R.C., 1990.

[EEHJ95] K. Eriksson, D. Estep, P. Hansbo, and C. Johnson. Introduction to numerical methods for differential equations. *Acta Numerica*, pages 105–158, 1995.

[GLLS97] M. Giles, M. Larson, M. Levenstam, and E. Süli. Adaptive error control for finite element approximations of the lift and drag coefficients in viscous flow. preprint NA-97/06, Comlab, Oxford University, 1997.

[God59] S. K. Godunov. A finite difference method for the numerical computation of discontinuous solutions of the equations of fluid dynamics. *Mat. Sb.*, 47:271–290, 1959.

[GP99] M. Giles and N.A. Pierce. Improved lift and drag estimates using adjoint Euler equations. Technical Report 99-3293, AIAA, Reno, NV, 1999.

[Har83] A. Harten. High resolution schemes for hyperbolic conservation laws. *J. Comp. Phys.*, 49:357–393, 1983.

[Har89] A. Harten. ENO schemes with subcell resolution. *J. Comp. Phys.*, 83:148–184, 1989.

[HH02] R. Hartmann and P. Houston. Adaptive discontinuous galerkin methods for the compressible euler equations. *J. Comp. Phys.*, 182(2):508–532, 2002.

[HOEC87] A. Harten, S. Osher, B. Engquist, and S. Chakravarthy. Uniformly high-order accurate essentially nonoscillatory schemes III. *J. Comp. Phys.*, 71(2):231–303, 1987.

[Joh87] C. Johnson. *Numerical Solution of Partial Differential Equations by the Finite Element Method*. Cambridge University Press, Cambridge, 1987.

[JP86] C. Johnson and J. Pitkäranta. An analysis of the discontinuous Galerkin method for a scalar hyperbolic equation. *Math. Comp.*, 46:1–26, 1986.

[JRB95] C. Johnson, R. Rannacher, and M. Boman. Numerics and hydrodynamics stability theory: towards error control in CFD. *SIAM J. Numer. Anal.*, 32:1058–1079, 1995.

[LB99] M.G. Larson and T.J. Barth. A posteriori error estimation for adaptive discontinuous Galerkin approximations of hyperbolic systems. In Cockburn, Karniadakis, and Shu, editors, *Discontinuous Galerkin Methods*, volume 11 of *Lecture Notes in Computational Science and Engineering*. Springer-Verlag, Heidelberg, 1999.

[OP99] J. T. Oden and S. Prudhomme. Goal-oriented error estimation and adaptivity for the finite element method. Technical Report 99-015, TICAM, U. Texas, Austin,TX, 1999.

[PO99] S. Prudhomme and J.T. Oden. On goal-oriented error estimation for elliptic problems: application to the control of pointwise errors. *Comp. Meth. Appl. Mech. and Eng.*, pages 313–331, 1999.

[RH73] W. H. Reed and T. R. Hill. Triangular mesh methods for the neutron transport equation. Technical Report LA-UR-73-479, Los Alamos National Laboratory, Los Alamos, New Mexico, 1973.

[S̈98] E. Süli. A posteriori error analysis and adaptivity for finite element approximations of hyperbolic problems. In Kröner, Ohlberger, and Rohde, editors, *An Introduction to Recent Developments in Theory and Numerics for Conservation Laws*, volume 5 of *Lecture Notes in Computational Science and Engineering*, pages 122–194. Springer-Verlag, Heidelberg, 1998.

[Van93] P. Vankeirsblick. *Algorithmic Developments for the Solution of Hyperbolic Conservation Laws on Adaptive Unstructured Grids*. PhD thesis, Katholieke Universiteit Leuven, Belgium, 1993.

[vL79] B. van Leer. Towards the ultimate conservative difference schemes V. A second order sequel to Godunov's method. *J. Comp. Phys.*, 32:101–136, 1979.